*Zeitschrift für anorganische und allgemeine Chemie*

Journal of Inorganic and General Chemistry
ZAAC
Zeitschrift für anorganische und allgemeine Chemie

RESEARCH ARTICLE OPEN ACCESS

# Delamination and Scrolling of the Phyllosilicate Kenyaite

Ingmar Pietsch[1] | Felix Uhlig[1] | Sabine Rosenfeldt[2] | Meike Kuhn[3] | Eva M. Herzig[3] | Josef Breu[1]

[1]Faculty of Biology, Chemistry & Earth Sciences, Chair of Inorganic Colloids for Electrochemical Energy Storage, University of Bayreuth, Bayreuth, Germany | [2]Faculty of Biology, Chemistry & Earth Sciences, Physical Chemistry 1 and Bavarian Polymer Institute, University of Bayreuth, Bayreuth, Germany | [3]Faculty of Mathematics, Physics & Computer Sciences, Dynamics and Structure Formation – Herzig Group, University of Bayreuth, Bayreuth, Germany

**Correspondence:** Josef Breu (josef.breu@uni-bayreuth.de)

**Received:** 18 December 2025 | **Revised:** 26 January 2026 | **Accepted:** 29 January 2026

**Keywords:** delamination | intercalation | kenyaite | morphology | nanoscrolls

## ABSTRACT

Kenyaite, $Na[Si_{10}O_{20}(OH)] \cdot 4H_2O$, is a phyllosilicate structurally related to Ilerite and Magadiite, whose platy, nonintergrown morphology makes it a promising precursor for high-aspect-ratio nanosheets. Here, Kenyaite is synthesized hydrothermally, fully exchanged with *N*-methyl-D-glucamine (meglumine), and delaminated via repulsive-osmotic 1D dissolution to yield monolayer silicate nanosheets of about 1.6 nm thickness and micrometer lateral dimensions without significant fracturing. X-ray diffraction, thermogravimetry, and spectroscopy confirm complete interlayer cation exchange, increased interlayer spacing, and preservation of the silicate framework, while light scattering and small-angle X-ray scattering demonstrate individual 2D objects that form nematic, lamellar liquid crystalline phases at high solids content. Upon dilution, the nanosheets spontaneously transform into nanoscrolls with a narrow width distribution and at most a few revolutions, as shown by atomic force microscopy and transmission electron microscopy, revealing scrolling steps consistent with the monolayer thickness. Comparison with Ilerite indicates that surface charge density, pH-dependent deprotonation, and nanosheet size can compensate for increased thickness, so that interfacial chemistry rather than stiffness alone governs the propensity and geometry of scrolling in this family of silicate nanosheets.

## 1 | Introduction

The standard approach for producing nanosheets is liquid phase exfoliation. As this processing method applies some kind of brute force, like ultrasonication, to a layered material with anisotropic but cohesive forces acting on adjacent monolayers, low yields, mediocre diameters, and broad thickness distributions are obtained [1, 2]. Contrary to this, with one-dimensional (1D) dissolution, interlayer chemistry is designed in a way that adjacent monolayers repel each other by Coulombic forces, and delamination is rendered a spontaneous, thermodynamically driven process. This process is gentle and allows the preparation of individual, highly anisotropic nanosheets with a large aspect ratio from a growing selection of layered materials [3]. To realize 1D dissolution, the forces acting between adjacent monolayers along the stacking direction of the crystal must be turned from cohesive to repulsive.

To reverse the interaction between stacked layers in the crystal from adhesive to repulsive, the interlayer space must first be substantially widened by swelling, allowing sufficient entropic freedom for interlayer species (counter ions and solvent). For instance, dipolar interactions of water with hydrophilic interlayer cations favor swelling. However, for most ionic compounds, especially those with high charge density, solvation enthalpy alone is insufficient to surpass the threshold where repulsion sets in. For instance, only low-charge clays ($<2\,e^-/nm^2$) in the Na-form spontaneously delaminate when immersed in water, while

In memory of Professor Rüdiger Kniep.

high-charge Na-vermiculite (>3 $e^-/nm^2$) experiences limited (crystalline) swelling due to discrete solvation of interlayer cations without triggering delamination [4]. The Na-forms of Ilerite and Kenyaite with layer charges of almost 4 $e^-/nm^2$ would fall in the range of nonswelling micas.

To allow for 1D dissolution, a subtle balance of solvation enthalpy, interlayer height, and charge density of the layers is required. Clearly, 1D dissolution becomes increasingly more difficult with increasing charge density of the layers, leading to stronger Coulomb attraction with interlayer cations. In these high-charge cases, swelling may; however, be supplemented by steric stress generated by bulky interlayer cations that help to increase the interlayer spacing beyond the threshold, where entropic contributions take over the bonding situation in the stack [5].

Intercalation of bulky and solvated counterions like *N*-Methyl-D-glucamin (meglumine, Meg) enables swelling of water into the interlayer space, increasing it against Coulomb forces. When this separation reaches a certain threshold value, interlayer cations separate into two diffuse double layers at both basal planes encompassing the interlayer space. The surface charge is partially shielded by the Helmholtz layer, while the entropic contribution increases, leading to repulsion between the sheets [6]. Solvent continues to enter, and the sheets dissolve unilaterally.

This gentle delamination route is reported for layered transition metal oxides [7, 8], clays [9], hydrous layer silicates (HLS) [10], and more [11]. With nanosheets carrying acidic—OH groups at basal surfaces, delamination by 1D dissolution often requires ion exchange with sterically demanding bases, like tetrabutylammonium hydroxide [7, 12] as the charge density for these compounds is controlled by the pH. For such compounds, Meg is a very good choice for an interlayer cation driving 1D dissolution as it is bulky, a strong base ($pK_a \sim 9.5$), and a rather hydrophilic amino sugar leading to high osmolalities and thus elevated osmotic pressures. Meg, therefore, successfully applied to delaminate lepidocrocite-type titanate and the HLS Ilerite (or RUB-18/octosilicate) in a single step [10, 13].

Once delaminated, individual nanosheets may be reassembled to monodomain films for gas membranes [14], or polymer composites [15] for barrier applications [10], or applied as carriers for photocatalysts [16, 17], or atomically thin coatings on active cathode materials [18].

Moreover, individual nanosheets are very flexible, allowing them to roll up, forming nanoscrolls (NS), which widens the range of potential applications [19–21]. Scrolling could be observed for various nanosheets. Scrolling can be forced by altering the surface energy on one basal plane, turning symmetrical hectorite nanosheets into Janus-type nanosheets. Similarly, the symmetry for double-layer hexaniobates and transition metal dichalcogenides may be broken by adsorption of surfactants or solvents on one of the two basal planes [22, 23]. Polar mono-layer hexaniobate sheets alleviate internal strain by scrolling [20]. The driving force becomes less obvious for centrosymmetric nanosheets like layered perovskites [21], titanates [24], and Ilerite [19, 25]. In particular, when the charge density is reduced, for instance by partial protonation of basal oxygen, which weakens repulsion between negatively charged basal surfaces, at some point back-folding becomes feasible, eventually triggering scrolling by intrasheet interactions.

While NS on their own are already of interest due to their anisotropy and altered physical and chemical properties [26–28], encasing nanoparticles allows for the introduction of additional functionalities [29–31].

Recently, Magadiite, a structural relative of Ilerite, was delaminated following the meglumine route, but only fractured nanosheets were obtained as the crystals of Magadiite were highly intergrown [32]. Herein, synthetic Kenyaite with a platy, nonintergrown morphology was synthesized and subsequently delaminated by 1D dissolution, resulting in 1.6 nm thick monolayers of appreciable aspect ratio. In concentrated suspensions, the obtained nanosheets are forced into a coplanar arrangement, yielding lamellar liquid crystals. Upon dilution, the nanosheets gain rotational freedom, and spontaneous scrolling sets in.

## 2 | Results and Discussion

### 2.1 | Crystal Structure

Kenyaite, $Na[Si_{10}O_{20}(OH)] \cdot 4H_2O$ (NaKeny), is a rare mineral first discovered in the caustic lake Magadii in Kenya, where it forms as a precursor to bedded cherts [33]. It is composed of $SiO_4$-tetrahedra, connected in sheets. At the basal surface, silanol groups are partially deprotonated, generating a negative charge that is compensated by hydrated $Na^+$-ions arranged in chains of edge-sharing octahedra. These chains are sandwiched between two four-membered cavities exposed at the corrugated basal planes (Figure 1) [34]. The three phyllosilicates Ilerite, Magadiite, and Kenyaite share this structural motif, only differing in their ratio of Na/Si, leading to increasing sheet thickness going from Ilerite to Magadiite and to Kenyaite from 0.7, 1.2, to 1.6 nm, respectively (Figure S1) [34–36].

### 2.2 | Synthesis

Kenyaite was synthesized following a slightly modified route published by Royer [37]. A dilute sol with a ratio of NaOH/$SiO_2$/$H_2O$ of 1/2/18 was crystallized at 150°C. The time varied from 3 to 5 days. After 3 days, Kenyaite has already formed, as evidenced by characteristic peaks observed in the powder X-ray diffractogram (PXRD). Longer reaction times sharpen the reflections, indicating increased crystallinity or crystal size, especially at 49.9 °(2$\theta$), corresponding to the in-plane (440) reflex.

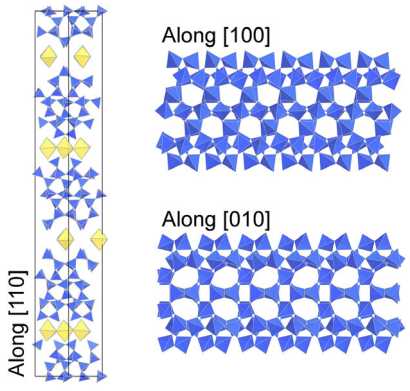


**FIGURE 1** | Crystal structure of Kenyaite, and structure of the layers as a 2 × 2 supercell.

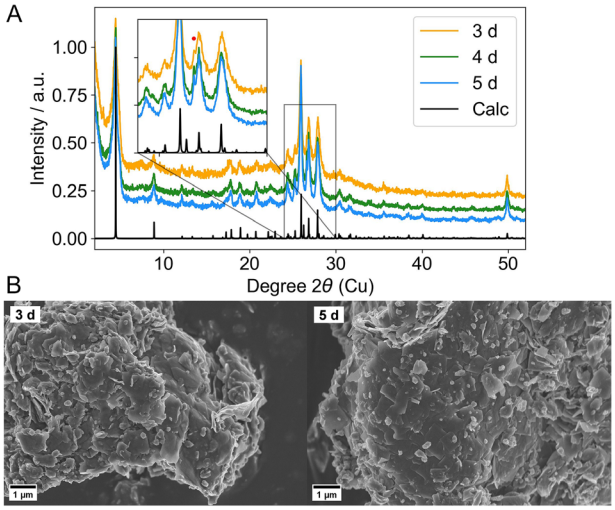


**FIGURE 2** | (A) PXRD of Kenyaites synthesized at 150°C with an inset showing a minute quartz side phase, denoted with a red dot. (B) SEM images of the products obtained after 3 and 5days.

At this stage, a small side phase of quartz appeared at 26.6 °(2$\theta$) (small red dot in the inset of Figure 2A), which becomes more prominent after more than 5 days (Figure S2). The formation of quartz was observed at shorter times than originally reported [37]. The faster occurrence of quartz is, however, in line with the results of Schwieger et al. working with a slightly more concentrated sol [38]. Scanning electron microscopy (SEM, Figures 2B, S4) showed dense aggregates in the range of 10 µm composed of sub-µm platelets. After 3 days, these crystallites appear frayed, eventually forming into platelets with better-defined edges after 4 to 5 days of ripening. After 5 days, platelets of varying morphology (rectangular and pseudo-hexagonal), with diameters of up to 1 µm and typical thicknesses below 50 nm, were obtained. The platy morphology with little to no perpendicular intergrowth is essential for delamination [39].

## 2.3 | Characterization of Suspensions and Individual Nanosheets

Complete cation exchange with $Meg^+$ was achieved by repeated (5×) change of the exchange solution (1 M of $Meg^+$). During subsequent washing, the ionic strength is lowered to the point (<0.02 M) where spontaneous delamination of MegKeny by 1D dissolution sets in. The yield of delaminated nanosheets suspended in the supernatant is ~ 65 wt%. The nondelaminated fraction was removed via centrifugation (4000 rpm for 10 min). Freeze-drying of the decanted nanosheet suspension yields a fine white powder. X-ray diffraction (Figure 3A) shows an increase in the *d*-spacing (001) from 19.9 to 23.0 Å due to bulky $Meg^+$ replacing hydrated $Na^+$ in the interlayer. The interlayer height of 7 Å is in good agreement with values reported for Ilerite and Magadiite intercalated with $Meg^+$ [10, 32]. Intraplane *hk*-bands confirm the structural integrity of the silicate layers, while (*hkl*) reflections are lost due to the turbostratic mode of restacking of the nanosheets upon drying the suspension. Energy dispersive X-ray spectroscopy (EDX, Table S1) could not detect remaining $Na^+$, confirming complete cation exchange. In the Infrared spectra (IR, Figure S3), the main difference is attributed to the removal of interlayer water coordinated to $Na^+$ that reduces the intensities at 3600 and 1630 $cm^{-1}$ [40]. Thermogravimetric analysis (TGA, Figure 3B) of NaKeny shows an initial loss of interlayer water of 9.9 wt% up to 150°C, followed by an additional 1.8 wt% weight loss from basal siloxane condensation [34]. For MegKeny, the removal of $Meg^+$ and siloxane condensation overlap. Based on the complete weight loss of 24.1 wt%, a chemical composition of $Meg_{0.94}H_{0.06}[Si_{10}O_{20}(OH)]$ can be deduced, confirming little surface protonation at pH 9, similar to what has been reported for Ilerite [10].

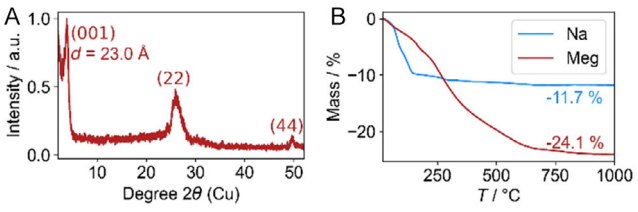


**FIGURE 3** | (A) PXRD of a freeze-dried MegKeny nanosheet suspension with denoted reflections. (B) TGA curves of NaKeny and MegKeny.

Successful delamination was cross-checked by static light scattering (SLS, Figure 4A) and small-angle X-ray scattering (SAXS, Figure 4B). In line with crystallite sizes observed by SEM (Figure 2B), the distribution of hydrodynamic radii of pristine NaKeny platelets as determined by SLS revealed an average diameter of 1.2 µm. A broad but single peak in the SLS indicates individual platelets in suspension and hence the absence of intergrown aggregates. Delamination only slightly decreases the value of the average hydrodynamic radii to 0.9 µm (aspect ratio of ~500), indicating that nanosheet fracturing during delamination may be neglected. SAXS intensities of concentrated suspensions (9.2 wt%) follow a $q^{-2}$ scaling, characteristic of scattering of 2D objects. Oscillations caused by coplanar nanosheets separated by a uniform distance, indicating a nematic phase, are weak but sufficient for interpretation. Fitting of the data to a lamellar model of circular disks representing the sheets with a thickness of 1.5 nm and a radius of 6 µm (beyond the resolution limit) results in a distance between sheets of 22 ± 3 nm at this concentration.

Samples for atomic force microscopy (AFM) were prepared by casting dilute suspensions (0.001 wt%) on silicon wafers that have been silylated with 3-aminopropyldimethylethoxysilane to create a positive surface charge. Only very few flat nanosheets were found (Figures S3 and 5A). They had a thickness of ~2.5 nm, which comprises the silicate thickness of 1.6 nm with hydrated $Meg^+$ adsorbed on the surface to balance charge. All but very few flat nanosheets were small with lateral dimensions of ~ 200 nm.

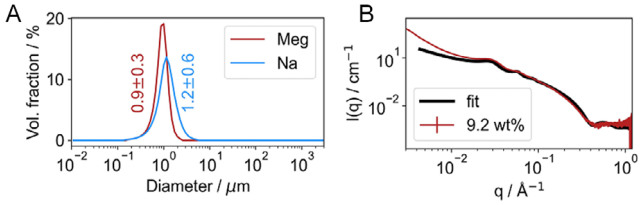


**FIGURE 4** | (A) Volumetric particle size distribution (hydrodynamic radii) as determined by SLS. (B) SAXS intensity of a concentrated suspension (9.2wt%) of MegKeny with a fit for a nematic phase (1.5 nm thick sheets of 6 µm radius with an intersheet distance of 22 nm).

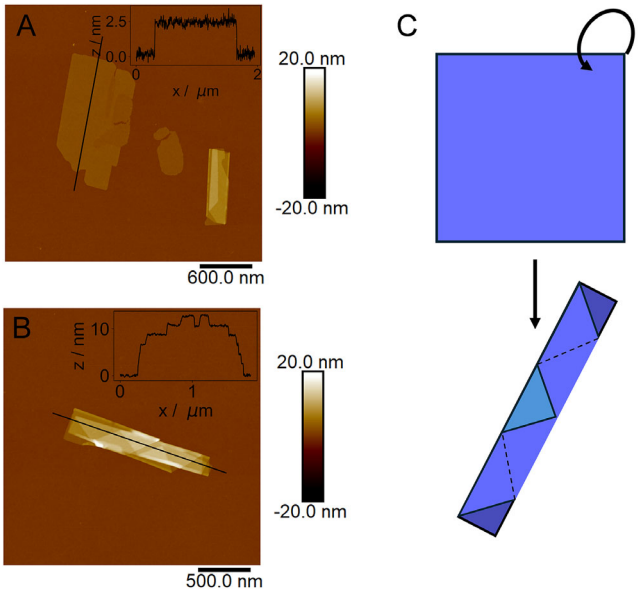


**FIGURE 5** | (A) AFM images of MegKeny nanosheets and a typical nanoscroll. (B) AFM image of a nanoscroll. (C) Proposed scrolling mechanism.

Most observed larger particles are fully scrolled nanosheets. They range in length from 0.2 to 1.2 µm, in width from 200 to 300 nm, and in height from 5 to 15 nm (Figures 5B, S5). For a tubular NS, width and height would be expected to be similar. We postulate that upon drying, the NS capillary forces trigger collapse of the lumen, leading to a flattening that increases width while minimizing height. We assume that the lumen of Ilerite scrolls also collapses upon drying, which was neither noted nor investigated by AFM at the time of publication.

Looking at the Kenyaite NS in more detail reveals individual scrolling steps of ~2 nm, approximately corresponding to the layer thickness. The steps indicate scrolling along a diagonal direction of the nanosheets (Figure 5C), contrary to Ilerite, where scrolling is observed along the sides of the square monolayers. Regarding potential reasons, we can only speculate. The anisotropic flexural moduli in this direction might be weak, leading to easier scrolling along one direction. Moreover, as the diagonal is longer than the side, intrasheet contacts triggering scrolling may be realized easier along the diagonal, particularly as Kenyaite nanosheets are smaller than Ilerite ones.

Even if scrolls form over a wide range of lengths, the widths are rather homogeneous, implying a stable minimal scrolling angle that a nanosheet can accommodate. This might also explain why small nanosheets remain flat. Given the minimal scrolling angle, they fail to fold back, interacting with the same nanosheet at the other end. We can only speculate why the few large nanosheets (Figure 5A) refrain from scrolling. Possibly, defects like fractures may hinder scrolling altogether. Even for long NS originating from large nanosheets, only 3 to 4 steps were observed by AFM. This indicates that NS would have a maximum of 2 to 3 scrolling revolutions and thus would be double to triple-walled tubes. The scrolling of nanosheets must put strain on chemical bonds. We therefore inspected IR spectra for differences and shifts triggered by scrolling. Significant changes in the spectra could, however, not be spotted (Figure S6).

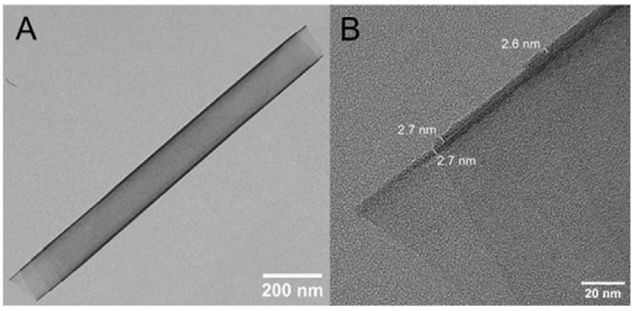


**FIGURE 6** | (A) TEM image of a NS. (B) Detail of the multilayered walls of the NS.

Transmission electron microscopy (TEM) confirms the formation of NS of ~200 nm width and micrometer lengths (Figures 6A, S7). Individual layers in the multiwall NS are well resolved at the tube ends. Zooming in allows us to estimate steps of approximately 2.7 nm (Figure 6B) again in decent agreement with the layer thickness.

The ease of scrolling is expected to be dependent on the stiffness of the nanosheet, which in turn should scale with thickness. We therefore expected a clear trend when going from Ilerite to Kenyaite as the layer thickness doubles with Kenyaite, while the structural motif of corner-sharing tetrahedra is preserved. The experiment, however, showed that Kenyaite scrolls as easily as Ilerite. The individual nanosheets of Ilerite indeed appear to be more flexible as the widths of NS of Ilerite (40 nm) are substantially smaller than that for Kenyaite (200 nm), indicating a smaller minimum scrolling angle for Ilerite. Acidity of the basal surfaces that in turn determines charge densities and the nanosheet extension; however, both have a crucial influence, masking or overruling the stiffness parameter. The smaller the surface charge and the larger the nanosheet, the more likely backfolding to the other end of the nanosheet will be. If scrolling is reversible, an increasing number of walls in the NS will shift the equilibrium toward NS. The interdependence of all these parameters does not allow a systematic variation that would allow conclusive statements on the likelihood and conditions that trigger or hamper scrolling.

## 3 | Conclusion

Kenyaite with a platy, nonintergrown morphology can be delaminated by 1D dissolution using meglumine to yield high-aspect-ratio, 1.6 nm thick nanosheets that retain the lateral dimensions and 2D crystalline order of the parent layered silicate. In concentrated suspensions, these nanosheets form lamellar liquid crystalline phases, while dilution induces spontaneous scrolling into NS with a narrow width distribution, limited wall number, and dimensions consistent with diagonal folding of the sheets. The observation that Kenyaite scrolls as readily as Ilerite with thinner monolayers, despite its higher layer thickness, underlines that surface charge density, pH-controlled deprotonation, and nanosheet extension can outweigh simple stiffness considerations in dictating the onset and geometry of scrolling. As dilution increases, the distance between individual nanosheets and thus gives them more freedom to bend, while at the same time the $OH^-$ concentration decreases by two orders of

magnitude, and concomitantly the surface charge decreases by protonation. Consequently, the electrostatic stabilization of nanosheets is weakened, and intrasheet self-interaction is fostered.

Overall, this work extends repulsive-osmotic 1D dissolution to Kenyaite, adds a new member to the family of spontaneously scrolling silicate nanosheets, and provides qualitative design rules for tuning delamination and scrolling in related layered materials via interlayer chemistry and surface acidity. Controlled scrolling will help to encase nanoparticles in different confinements, depending on whether Ilerite or Kenyaite is used. Strictly working at high concentrations, scrolling may be prevented for Kenyaite. This will allow preparation of monodomain films with anisotropic properties, like distinct thermal conductivities in- and cross-plane. Comparison of thermal conductivities of films of Ilerite and Kenyaite may eventually allow fundamental insights into the causes of thermal anisotropy. Work in this direction is in progress.

## 4 | Experimental Section

### 4.1 | Synthesis and Delamination of Kenyaite

Kenyaite was synthesized as described in the literature [37]. 150.0 g of Köstrosol (30 wt% $SiO_2$, Chemiewerke Köstritz, 1030 KD), 16.5 g of double-distilled water, and 15.0 g of NaOH (fishersci) were stirred overnight at room temperature (RT). The clear sol was transferred into teflon-lined steel autoclaves (66 % filling factor) and aged at 150°C for 3 to 5 d and subsequently washed with water to a pH of 9 via centrifugation. A small part was dried at RT for analysis, and the rest was stored wet to prevent interparticle condensation [39]. Between runs, the teflon inlets were cleaned with 1 M NaOH at 100°C. 800 mg of the wet product was shaken in 25 mL of a 1 M solution of meglumine (thermofisher) that was titrated with HCl (conc., Grüssing) to a pH of 9. The exchange solution was replaced every 8/16 h for a total of 5 exchanges. Washing with 25 ml of water 5 times lowered the ionic strength and triggered delamination. Nondelaminated aggregates were removed by centrifugation at 4000 rpm for 10 min. The supernatant suspension was concentrated at 10 000 rpm for 15 min. The solid content of the suspensions was determined by drying small aliquots at 100°C overnight in a teflon dish.

### 4.2 | Analysis

Powders were ground with agate mortars and packed in 0.5 mm capillaries (Hilgenberg). XRDs were measured on a STOE STADI P diffractometer operated with Cu $K_{\alpha 1}$ radiation ($\lambda = 1.54056$ Å) and a linear position-sensitive Dectris MYTHEN 1K detector.

SEM was performed on a ZEISS Ultra Plus, while EDX was performed on a ZEISS Leo 1530. For TEM, a suspension diluted to 0.0001 wt% was drop cast on a Cu 200 mesh with a Formvar/Carbon film and analyzed in a JEOL JEM-2200FS.

A Linseis STA PT 1600 was used for TGA, applying synthetic air up to 1000°C with a rate of 5°C/min.

IR were measured in attenuated total reflection Fourier transform mode on a Bruker IFS66v.

For SLS, dilute suspensions were measured on a LA-950 from HORIBA, and a refractive index of 1.45 for the silicate was assumed.

A Xenocs Xeuss 3.0 with GeniX 3D Cu High Flux Very Long Focus source ($\lambda = 1.5418$ Å) and a Dectris Eiger2 R 1 M detector was used for SAXS measurements. The detector contains $1028 \times 1062$ pixels at $75 \times 75$ µm and is positioned 0.2, 0.75, and 1.8 m from the samples. Samples were measured with a $0.5 \times 0.5$ mm beam size for 900–1800 s (depending on detector position) under vacuum. 1D data were generated with the software of the instrument (XSACT, including normalization to roi of interest). Suspensions of MegKeny were concentrated via centrifugation, washed with a solution of 50 mM Meg to increase the ionic background, then again centrifuged at 14 500 rpm for 30 min and filled into 1 mm capillaries (Hilgenberg) for SAXS. The scattering intensity of a water-filled capillary was used for background correction. Further evaluation was done by the software SAXSutilities [41] or scatter [42].

For AFM, Si wafers were cleaned via snow jet, plasma treated, and silylated with 3-aminopropyldimethyl-ethoxysilane (abcr) under vacuum overnight. Dispersions of MegKeny (0.001 wt%) were drop cast and left to dry at RT. The measurements were performed on a Bruker Dimension Icon with a NanoScope V controller and a ScanAsyst-Air silicon tip in PeakForce mode. Images were analyzed with NanoScope Analysis 1.8.

Crystal structures were visualized with VESTA [43].

#### Acknowledgments

The authors would like to acknowledge Marco Schwarzmann for measuring SEM and TEM, and Michael Thelen for measuring AFM. The authors gratefully acknowledge the support and funding by the German Research Foundation (DFG) within CRC 1585 (project number 492723217) for subprojects C01 and B03. Support from the keylabs (Mesoscale Characterization: Scattering Techniques, Surface and Interface Characterization, and Electron and Optical Microscopy) of the Bavarian Polymer Institute (BPI) at the University of Bayreuth is much appreciated. The use of DFG INST91/443-1 (438562776) is acknowledged.

Open Access funding enabled and organized by Projekt DEAL.

#### Funding

This work was supported by Deutsche Forschungsgemeinschaft (492723217, 438562776).

#### Conflicts of Interest

The authors declare no conflicts of interest.

#### Data Availability Statement

The data that support the findings of this study are available from the corresponding author upon reasonable request.

#### References

1. R. Ma and T. Sasaki, "Two-Dimensional Oxide and Hydroxide Nanosheets: Controllable High-Quality Exfoliation, Molecular Assembly, and Exploration of Functionality," *Accounts of Chemical Research* 48 (2015): 136–143.

2. R. Ma and T. Sasaki, "Nanosheets of Oxides and Hydroxides: Ultimate 2D Charge-Bearing Functional Crystallites," *Advanced Materials* 22 (2010): 5082–5104.

3. V. Dudko, O. Khoruzhenko, S. Weiß, et al., "Repulsive Osmotic Delamination: 1D Dissolution of 2D Materials," *Advanced Materials Technologies* 8 (2023): 2200553.

4. M. Daab, S. Rosenfeldt, H. Kalo, et al., "Two-Step Delamination of Highly Charged, Vermiculite-Like Layered Silicates via Ordered Heterostructures," *Langmuir* 33 (2017): 4816–4822.

5. M. Daab, N. J. Eichstaedt, A. Edenharter, S. Rosenfeldt, and J. Breu, "Layer Charge Robust Delamination of Organo-Clays," *RSC Advances* 8 (2018): 28797–28803.

6. S. Rosenfeldt, M. Stöter, M. Schlenk, et al., "In-Depth Insights into the Key Steps of Delamination of Charged 2D Nanomaterials," *Langmuir* 32 (2016): 10582–10588.

7. T. Sasaki and M. Watanabe, "Osmotic Swelling to Exfoliation. Exceptionally High Degrees of Hydration of a Layered Titanate," *Journal of the American Chemical Society* 120 (1998): 4682–4689.

8. R. E. Schaak and T. E. Mallouk, "Perovskites by Design: A Toolbox of Solid-State Reactions," *Chemistry of Materials* 14 (2002): 1455–1471.

9. M. Stöter, D. A. Kunz, M. Schmidt, et al., "Nanoplatelets of Sodium Hectorite Showing Aspect Ratios of ≈20 000 and Superior Purity," *Langmuir* 29 (2013): 1280–1285.

10. P. Loch, D. Schuchardt, G. Algara-Siller, et al., "Nematic Suspension of a Microporous Layered Silicate Obtained by Forceless Spontaneous Delamination via Repulsive Osmotic Swelling for Casting High-Barrier All-Inorganic Films," *Science Advances* 8 (2022): eabn9084.

11. H. Ding, S. T. Khan, K. N. Aguirre, et al., "Exfoliation of $\alpha$-Zirconium Phosphate Using Tetraalkylammonium Hydroxides," *Inorganic Chemistry* 59 (2020): 7822–7829.

12. K. Awaya, K. Sekiguchi, H. Kitagawa, S. Yamada, and S. Ida, "Preparation of Silicate Nanosheets by Delaminating RUB-18 for Transparent, Proton Conducting Membranes," *Chemical Communications* 57 (2021): 6304–6307.

13. G. Cha, S. Weiß, J. Thanner, et al., "Gentle, Spontaneous Delamination of Layered Titanate Yielding New Types of Lithium Titanate Nanosheets," *Chemistry of Materials* 35 (2023): 7208–7217.

14. M. Dakhchoune, L. F. Villalobos, R. Semino, et al., "Gas-Sieving Zeolitic Membranes Fabricated by Condensation of Precursor Nanosheets," *Nature Materials* 20 (2021): 362–369.

15. M. Röhrl, L. K. S. Federer, R. L. Timmins, et al., "Disorder–Order Transition—Improving the Moisture Sensitivity of Waterborne Nanocomposite Barriers," *ACS Applied Materials & Interfaces* 13 (2021): 48101–48109.

16. T. Oshima, D. Lu, and K. Maeda, "Preparation of Pt-Intercalated $KCa_2Nb_3O_{10}$ Nanosheets and Their Photocatalytic Activity for Overall Water Splitting," *Chemnanomat* 2 (2016): 748–755.

17. C. Fukasawa, T. Takei, S. Yanagida, and N. Kumada, "Preparation of $KCa_2Nb_3O_{10}$-Based Porous Hybrid with Ru for $H_2$ Generation Catalyst by $NH_3$ Decomposition," *Journal of the Ceramic Society of Japan* 128 (2020): 912–917.

18. M. Stevenson, S. Weiß, G. Cha, et al., "Osmotically Delaminated Silicate Nanosheet-Coated NCM for Ultra-Stable $Li^+$ Storage and Chemical Stability Toward Long-Term Air Exposure," *Small* 19 (2023): 2302617.

19. Y. Asakura, M. Sugihara, T. Hirohashi, et al., "Formation of Silicate Nanoscrolls through Solvothermal Treatment of Layered Octosilicate Intercalated with Organoammonium Ions," *Nanoscale* 11 (2019): 12924–12931.

20. G. B. Saupe, C. C. Waraksa, H.-N. Kim, et al., "Nanoscale Tubules Formed by Exfoliation of Potassium Hexaniobate," *Chemistry of Materials* 12 (2000): 1556–1562.

21. R. E. Schaak and T. E. Mallouk, "Prying Apart Ruddlesden–Popper Phases: Exfoliation into Sheets and Nanotubes for Assembly of Perovskite Thin Films," *Chemistry of Materials* 12 (2000): 3427–3434.

22. T. Harada, Y. Suzuki, T. Nakato, J. Breu, and J. Kawamata, "Real-Time Monitoring of Adsorption-Induced Scrolling of Colloidal Inorganic Nanosheets," *Langmuir* 40 (2024): 9189–9196.

23. X. Cui, Z. Kong, E. Gao, et al., "Rolling up Transition Metal Dichalcogenide Nanoscrolls via One Drop of Ethanol," *Nature Communications* 9 (2018): 1301.

24. R. Ma, Y. Bando, and T. Sasaki, "Directly Rolling Nanosheets into Nanotubes," *The Journal of Physical Chemistry B* 108 (2004): 2115–2119.

25. F. Uhlig, I. Pietsch, A. Stich, et al., "Quantitative Scrolling into Microporous Nanotubes of the Hydrous Layered Silicate Ilerite," *Zeitschrift für Anorganische Und Allgemeine Chemie* 650 (2024): e202400002.

26. M. C. F. Costa, P. R. Ng, S. Grebenchuck, et al., "Colossal Enhancement of Electrical and Mechanical Properties of Graphene Nanoscrolls," *Carbon* 208 (2023): 140–147.

27. S. Aftab, M. Z. Iqbal, and Y. S. Rim, "Recent Advances in Rolling 2D TMDs Nanosheets into 1D TMDs Nanotubes/Nanoscrolls," *Small* 19 (2023): 2205418.

28. Z. Liu, J. Gao, G. Zhang, Y. Cheng, and Y.-W. Zhang, "From Two-Dimensional Nano-Sheets to Roll-up Structures: Expanding the Family of Nanoscroll," *Nanotechnology* 28 (2017): 385704.

29. R. Ma, Y. Kobayashi, W. J. Youngblood, and T. E. Mallouk, "Potassium Niobate Nanoscrolls Incorporating Rhodium Hydroxide Nanoparticles for Photocatalytic Hydrogen Evolution," *Journal of Materials Chemistry* 18 (2008): 5982–5985.

30. S. Adireddy, C. E. Carbo, T. Rostamzadeh, J. M. Vargas, L. Spinu, and J. B. Wiley, "Inside Back Cover: Peapod-Type Nanocomposites through the In Situ Growth of Gold Nanoparticles Within Preformed Hexaniobate Nanoscrolls (Angew. Chem. Int. Ed. 18/2014)," *Angewandte Chemie International Edition* 53 (2014): 4725–4725.

31. Y.-C. Chen, Y.-K. Hsu, R. Popescu, D. Gerthsen, Y.-G. Lin, and C. Feldmann, "Au@Nb@H x K1-xNbO3 Nanopeapods with Near-Infrared Active Plasmonic Hot-Electron Injection for Water Splitting," *Nature Communications* 9 (2018): 232.

32. S. Hasebe, M. Yatomi, N. Hori, T. Iwakami, T. Matsuno, and A. Shimojima, "Hierarchically Porous Materials via Co-Assembly of Exfoliated Layered Silicate with Mesoporous Silica Nanoparticles," *Langmuir* 41 (2025): 25954–25961.

33. H. P. Eugster, "Hydrous Sodium Silicates from Lake Magadi, Kenya: Precursors of Bedded Chert," *Science* 157 (1967): 1177–1180.

34. B. Marler, I. Grosskreuz, and H. Gies, "The Crystal Structure of Synthetic kenyaite, Na2Si20O40(OH)2·8H2O," *Journal of Solid State Chemistry* 300 (2021): 122215.

35. Yşar Krysiak, M. Maslyk, B. N.ádia Silva, et al., "The Elusive Structure of Magadiite, Solved by 3D Electron Diffraction and Model Building," *Chemistry of Materials* 33 (2021): 3207–3219.

36. S. Vortmann, J. Rius, S. Siegmann, and H. Gies, "Ab Initio Structure Solution from X-Ray Powder Data at Moderate Resolution: Crystal Structure of a Microporous Layer Silicate," *The Journal of Physical Chemistry B* 101 (1997): 1292–1297.

37. B. Royer, N. F. Cardoso, E. C. Lima, V. S. O. Ruiz, T. D.;s R. Macedo, and C. Airoldi, "Organofunctionalized kenyaite for Dye Removal from Aqueous Solution," *Journal of Colloid and Interface Science* 336 (2009): 398–405.

38. W. Schwieger, W. Heyer, F. Wolf, and K. H. Bergk, "Zur Synthese Von Kristallinen Metallsilicathydraten Mit Schichtstruktur," *Zeitschrift für Anorganische Und Allgemeine Chemie* 548 (1987): 204–216.

39. Y. Bi, J.-F. Lambert, Y. Millot, et al., "Relevant Parameters for Obtaining High-Surface Area Materials by Delamination of Magadiite, a Layered Sodium Silicate," *Journal of Materials Chemistry* 21 (2011): 18403–18411.

40. Y. Huang, Z. Jiang, and W. Schwieger, "Vibrational Spectroscopic Studies of Layered Silicates," *Chemistry of Materials* 11 (1999): 1210–1217.

41. M. Sztucki, *SAXSutilities, A Graphical User Interface for Processing and Analysis of Small Angle X-ray Scattering Data,* 1.024 ed., Zenodo, (2021), https://doi.org/10.1002/zaac.202500182.

42. S. Förster, S. Fischer, K. Zielske, et al., "Calculation Of Scattering-patterns Of Ordered Nano-and Mesoscale Materials," *Advances in Colloid and Interface Science* 163 (2011): 53–83.

43. K. Momma and F. Izumi, "VESTA 3 for Three-Dimensional Visualization of Crystal, Volumetric and Morphology Data," *Journal of Applied Crystallography* 44 (2011): 1272–1276.

## Supporting Information

Additional supporting information can be found online in the Supporting Information section. **Supporting Fig. S1:** Crystal structures of Ilerite, Magadiite, and Kenyaite. **Supporting Fig. S2:** PXRD of NaKeny after 6 d at 150°C with a red dot denoting the quartz side phase. **Supporting Fig. S3:** FTIR of NaKeny and freeze-dried MegKeny nanosheets. **Supporting Fig. S4:** SEM images of synthesized NaKeny at 150°C. **Supporting Fig. S5:** AFM overview of MegKeny particles. **Supporting Fig. S6:** FTIR spectra of freezedried MegKeny as sheets and a freezedried suspension of scrolls, that had been diluted to trigger scrolling and reconcentrated via centrifugation. **Supporting Fig. S7:** TEM image of multiple nanoscrolls and detail of a thicker scroll. **Supporting Table S1:** Composition of MegKeny in atom%, sputtered with Carbon.